Supplement of Atmos. Meas. Tech., 17, 5821–5839, 2024
https://doi.org/10.5194/amt-17-5821-2024-supplement

Atmospheric Measurement Techniques
Open Access
EGU

Supplement of

Development and deployment of a mid-cost CO_2 sensor monitoring network to support atmospheric inverse modeling for quantifying urban CO_2 emissions in Paris

Jinghui Lian et al.

Correspondence to: Jinghui Lian (jinghui.lian@suez.com) and Olivier Laurent (olivier.laurent@lsce.ipsl.fr)

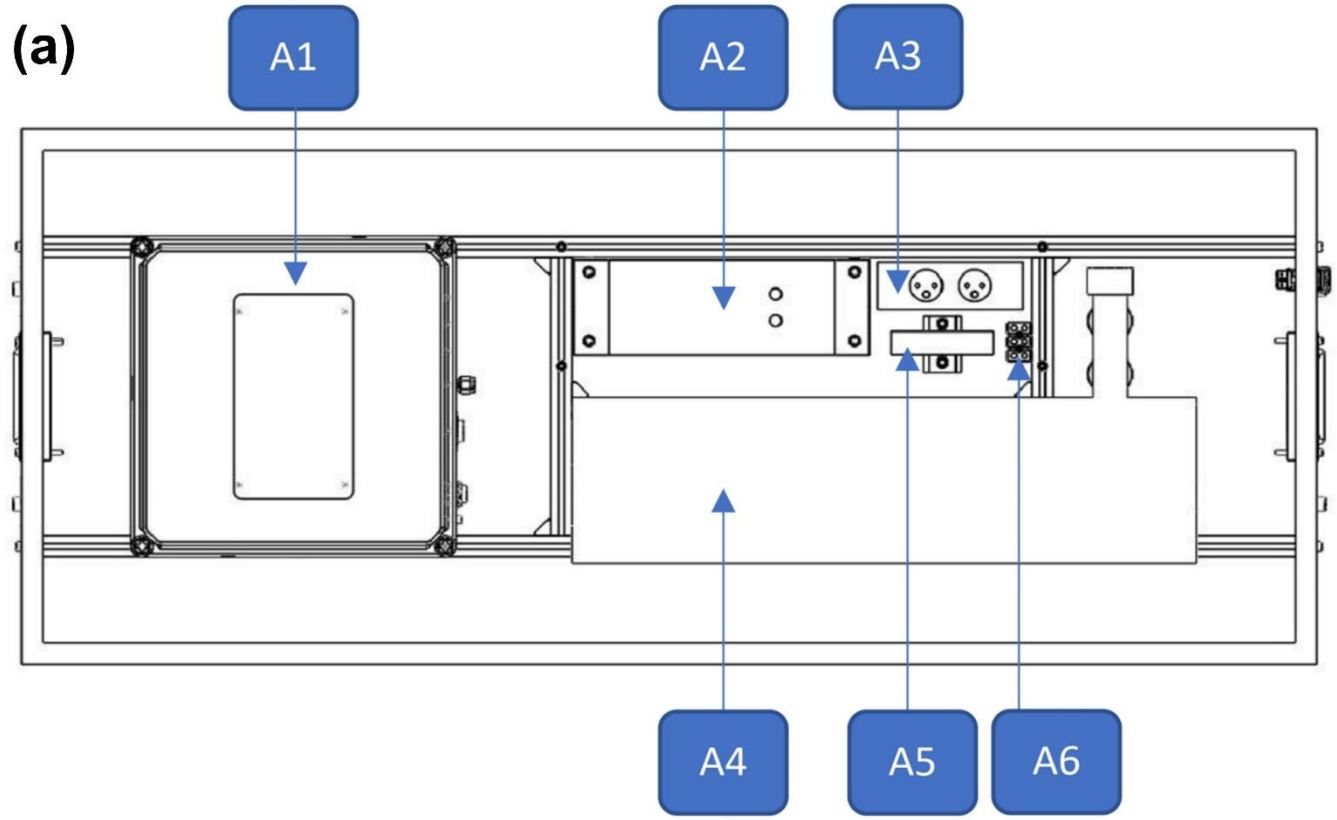

	Item	Description
A1	Slot for HPP sensor box	The HPP sensor box is installed by affixing it with four threaded screws
A2	Slot for flushing pump	Optional
A3	Power strips	Slot 1: HPP sensor box. Slot 2: flushing pump
A4	Slot for target gas container	5L tank
A5	12V power supply	For supplying the container fans
A6	Terminal block	The connection to the electrical network is done from here

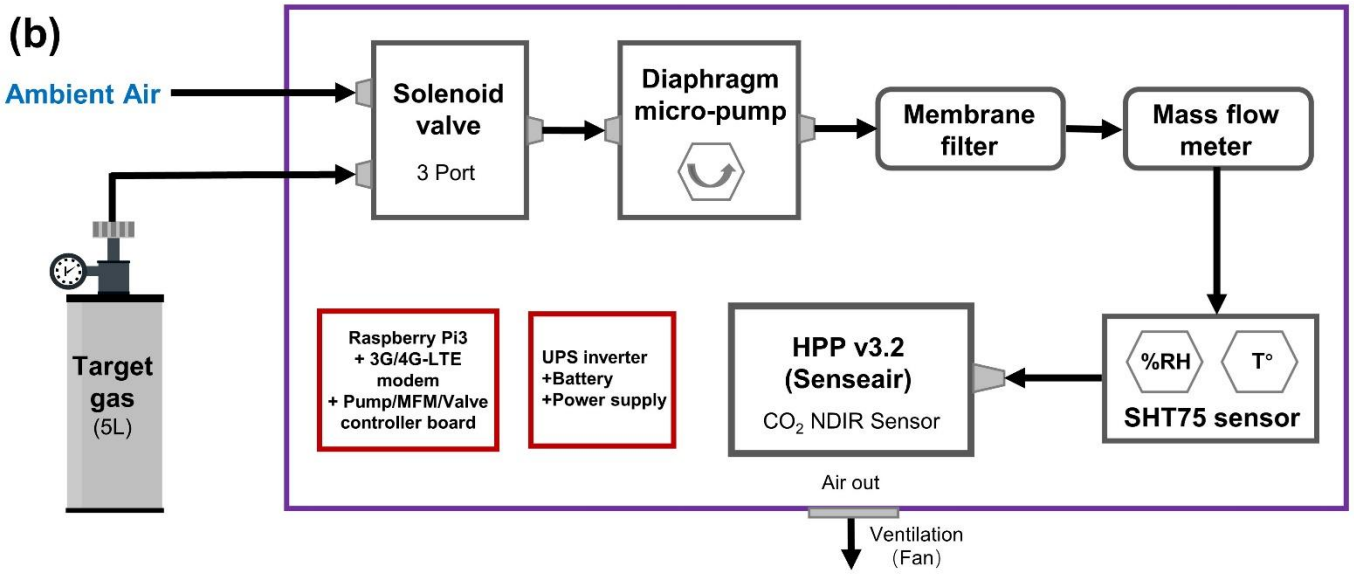

Figure S1. (a) Schematic of the integrated HPP CO_2 instrument for the field deployment, (b) Plumbing design of the airflow inside the integrated HPP sensor box, as shown in Figure 1b and located at A1 in (a). Figure (a) was made by © Eloneo (https://eloneo.fr/)

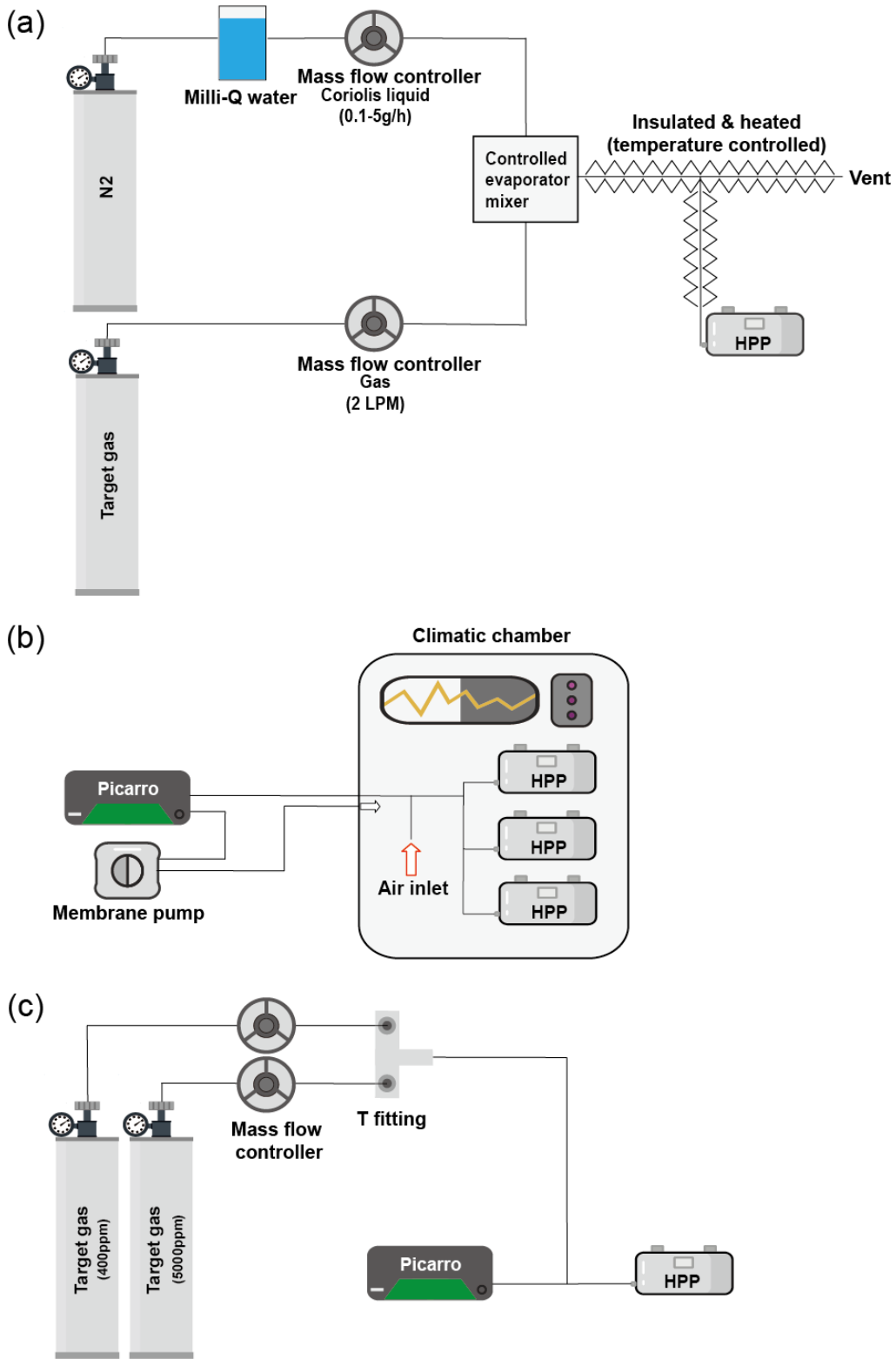

Figure S2. Schematic of the HPP laboratory (a) water vapor sensitivity test, (b) pressure and temperature sensitivity tests and (c) CO_2 sensitivity test for the calibration procedure. Note that all 8 HPP instruments have been subjected to these tests.

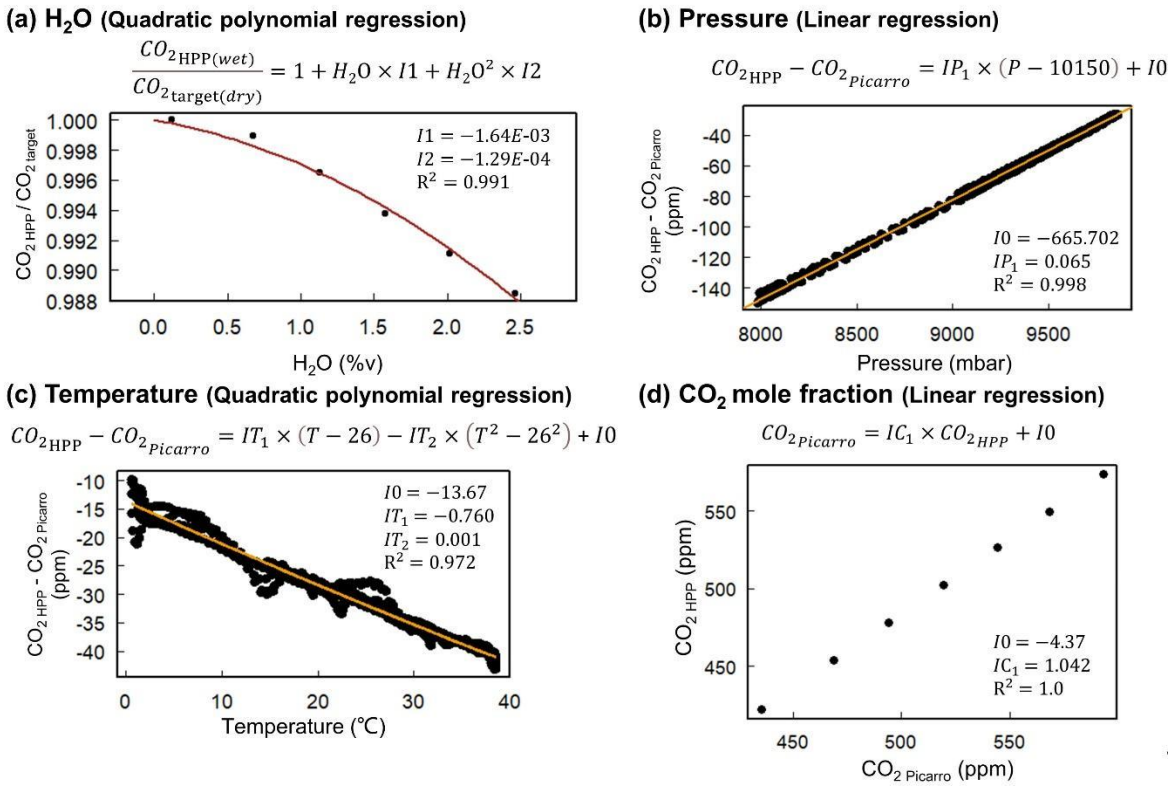

Figure S3. Relationships between the raw 1-minute averaged CO_2 mole fraction reported by one of the HPP sensors (HPP3) and variations in H_2O, T, P and CO_2 mole fraction in the sensitivity tests, respectively. The derived regression coefficients are used in the CO_2 calibration equation.

Section S1

To mitigate delays in sensor responses and ensure stability, thorough CO_2 flushing of the sensor cell is necessary. During the CO_2 correction coefficient IC_1 determination process, we sequentially sampled CO_2 mole fraction for a duration of 10 minutes, with 7 minutes dedicated to flushing and only the last 3 minutes of data used. During the on-site daily target gas injection for the $CO_{2_{offset}}$ calculation, we sampled CO_2 mole fraction for a duration of 3 minutes, with 2 minutes of flushing and only the last minute of data used.

The differences in flushing times are due to two reasons. First, the CO_2 correction coefficient IC_1 is determined through a multipoint CO_2 regression using the seven mole fraction values assigned within the 400-600 ppm range. Conversely, the CO_2 concentration in the target tank (which contains dry compressed natural air, pressurized at 200 bars and calibrated in CO_2) is supposed to be close to the ambient air CO_2 concentration on-site during midday. The step between two different CO_2 concentrations in the IC_1 determination process is greater than that during the target tank injection for drift correction, thus requiring a longer flushing time to achieve stabilization. Second, the CRDS and the mid-cost HPP sensor do not measure at the same flow rate, approximately 0.25 LPM for the CRDS and about 1 LPM for the HPP. They also have different precision targets. The CRDS sensor requires an extended period of target gas measurements to achieve a stability of less than 0.05 ppm, which is suitable for applications beyond this specific

intercomparison. Therefore, the flushing time in the IC_1 determination process, when the HPP sensor measures in parallel with the CRDS, is expected to be longer.

Before implementing this setting, we carried out several sensitivity tests on the sensor performance with a daily injection of target gas lasting 5 minutes at LSCE laboratory. Figure S4 shows the evolution of target gas injection duration in relation to the differences in CO_2 concentration between the other 4 minutes and the 3rd minute at one HPP sensor (HPP3) over 26 days. It demonstrates that a 3-minute target gas injection, specifically utilizing the 3rd minute data, proved to be sufficient. The added value of the 4th- and 5th- minute injection is rather limited. Therefore, the choice of a two-minute flush serves as a good compromise between maintaining good sensor performance (ensuring a target accuracy of 1 ppm) and minimizing gas consumption (thereby extending the lifespan of the tank and reducing associated maintenance requirements).

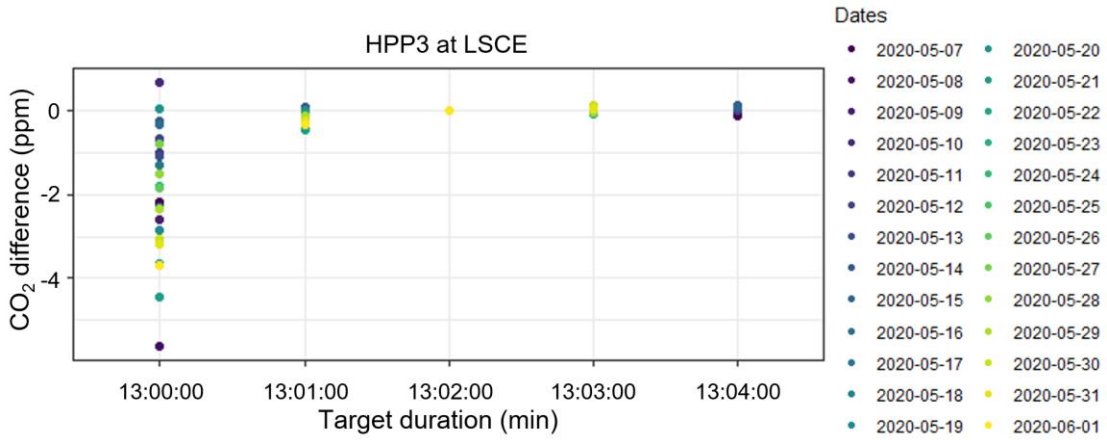

Figure S4. The evolution of target gas injection duration in relation to the differences in CO_2 concentration between the other 4 minutes and the 3rd minute at one HPP sensor (HPP3), with a daily injection of target gas lasting 5 minutes over 26 days at LSCE.

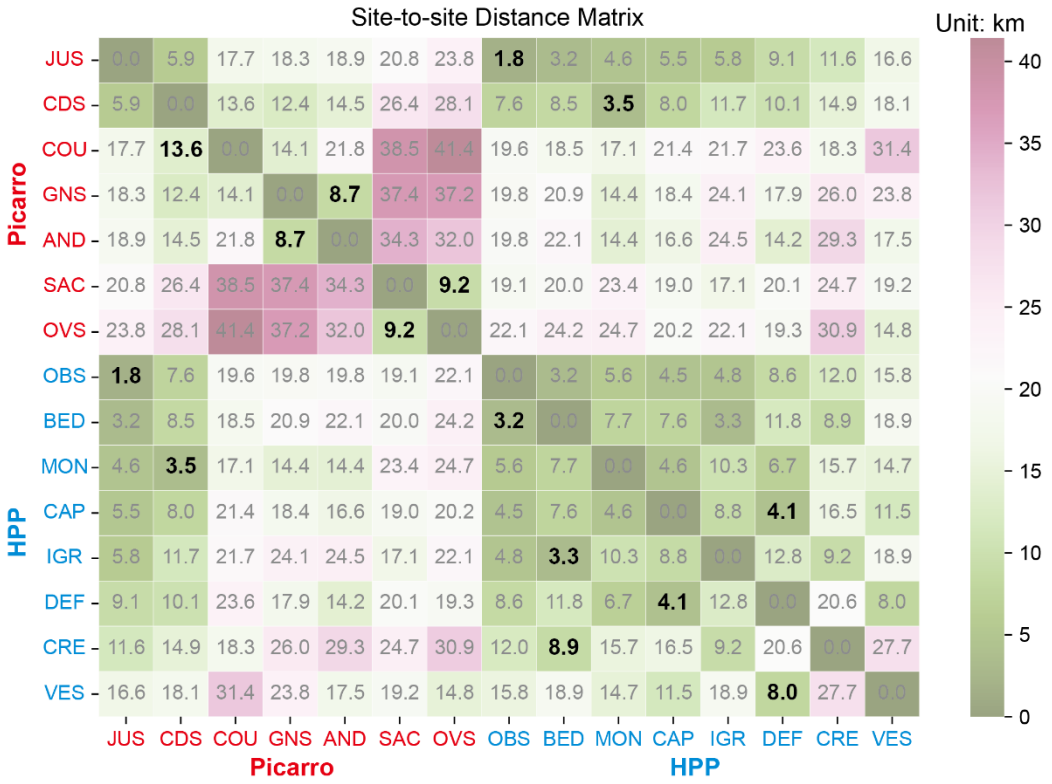

Site (km)	JUS	CDS	COU	GNS	AND	SAC	OVS	OBS	BED	MON	CAP	IGR	DEF	CRE	VES	Average
Picarro	5.9	5.9	13.6	8.7	8.7	9.2	9.2									**8.7**
HPP								3.2	3.2	4.6	4.1	3.3	4.1	8.9	8	**4.9**
Picarro +HPP	1.8	3.5	13.6	8.7	8.7	9.2	9.2	1.8	3.2	3.5	4.1	3.3	4.1	8.9	8	**6.1**

Figure S5. Site-to-site distance in kilometers. The distances to the nearest site for each site are highlighted in bold black font (read by rows) and are summarized in the table.

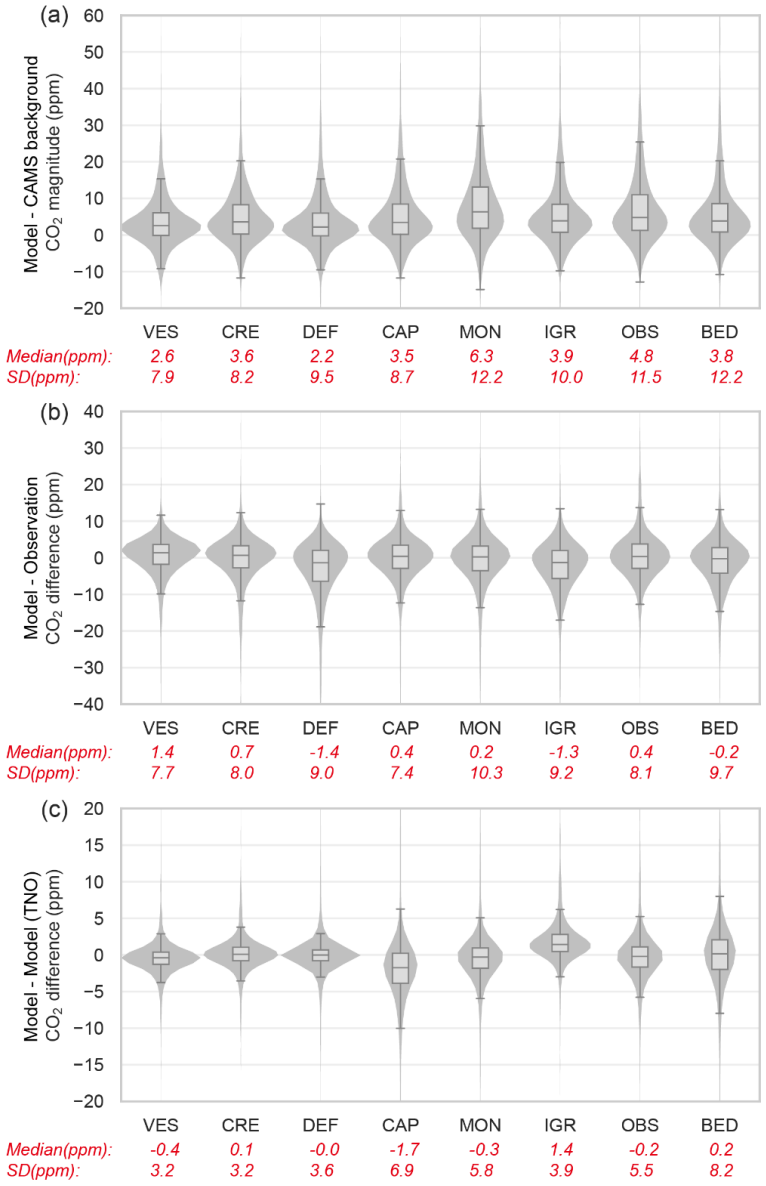

Figure S6. (a) Distribution of the local hourly afternoon (12-17 UTC) CO_2 signals at each HPP station from July 2020 to December 2022. This is computed by using the WRF-Chem simulated total CO_2 (fossil fuel, biogenic, and background sources) minus the background CO_2 mole fractions derived from the CAMS dataset. (b) Distribution of the differences in hourly afternoon CO_2 mole fraction between the WRF-Chem model and the observations at each HPP station from July 2020 to December 2022. (c) Distribution of the differences in simulated hourly afternoon CO_2 mole fraction, using Origins.earth (default) and TNO 1km inventory (Dellaert et al., 2019) as fossil fuel CO_2 emission inputs for the WRF-Chem model respectively. This model sensitivity test was carried out for the year 2018 (Lian et al., 2023). The midpoint, the box and the whiskers represent the 0.5 quantile, 0.25/0.75 quantiles, and 0.1/0.9 quantiles respectively.

SI Reference:

Dellaert S., Super I., Visschedijk A., Denier van der Gon H.A.C.: High resolution scenarios of CO_2 and CO emissions. https://www.che-project.eu/sites/default/files/2019-05/CHE-D4-2-V1-0.pdf, 2019.

Lian, J., Lauvaux, T., Utard, H., Bréon, F.-M., Broquet, G., Ramonet, M., Laurent, O., Albarus, I., Chariot, M., Kotthaus, S., Haeffelin, M., Sanchez, O., Perrussel, O., Denier van der Gon, H. A., Dellaert, S. N. C., and Ciais, P.: Can we use atmospheric CO_2 measurements to verify emission trends reported by cities? Lessons from a 6-year atmospheric inversion over Paris, Atmos. Chem. Phys., 23, 8823–8835, https://doi.org/10.5194/acp-23-8823-2023, 2023.

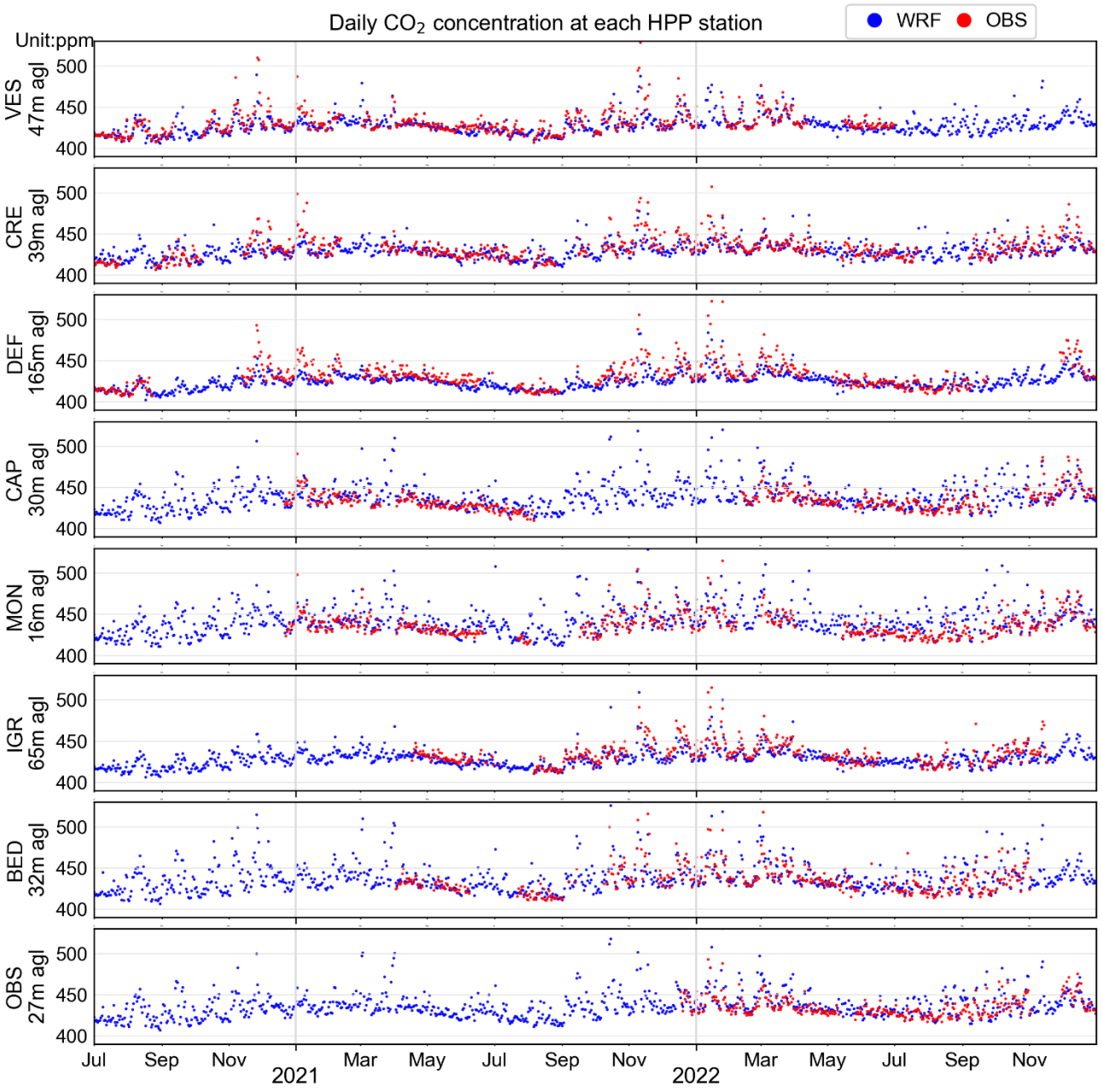

Figure S7. Time series of the modeled and observed daily CO_2 concentration at each HPP station.

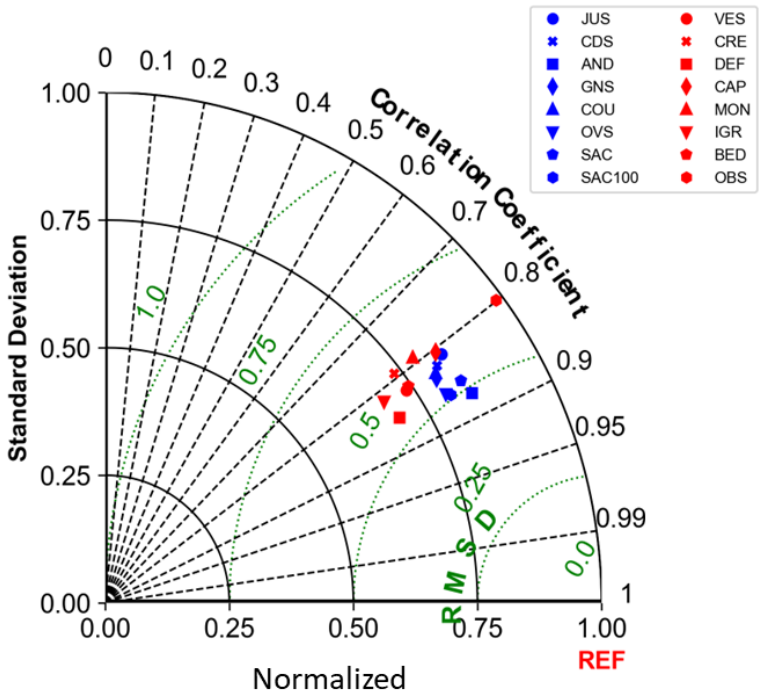

Figure S8. Comparisons of the observed and modeled hourly afternoon (12-17 UTC) CO_2 mole fractions at 7 CRDS and 8 HPP stations over the period of July 2020 to December 2022. The SAC station has two air inlets placed at 15 m and 100 m above ground level, respectively.

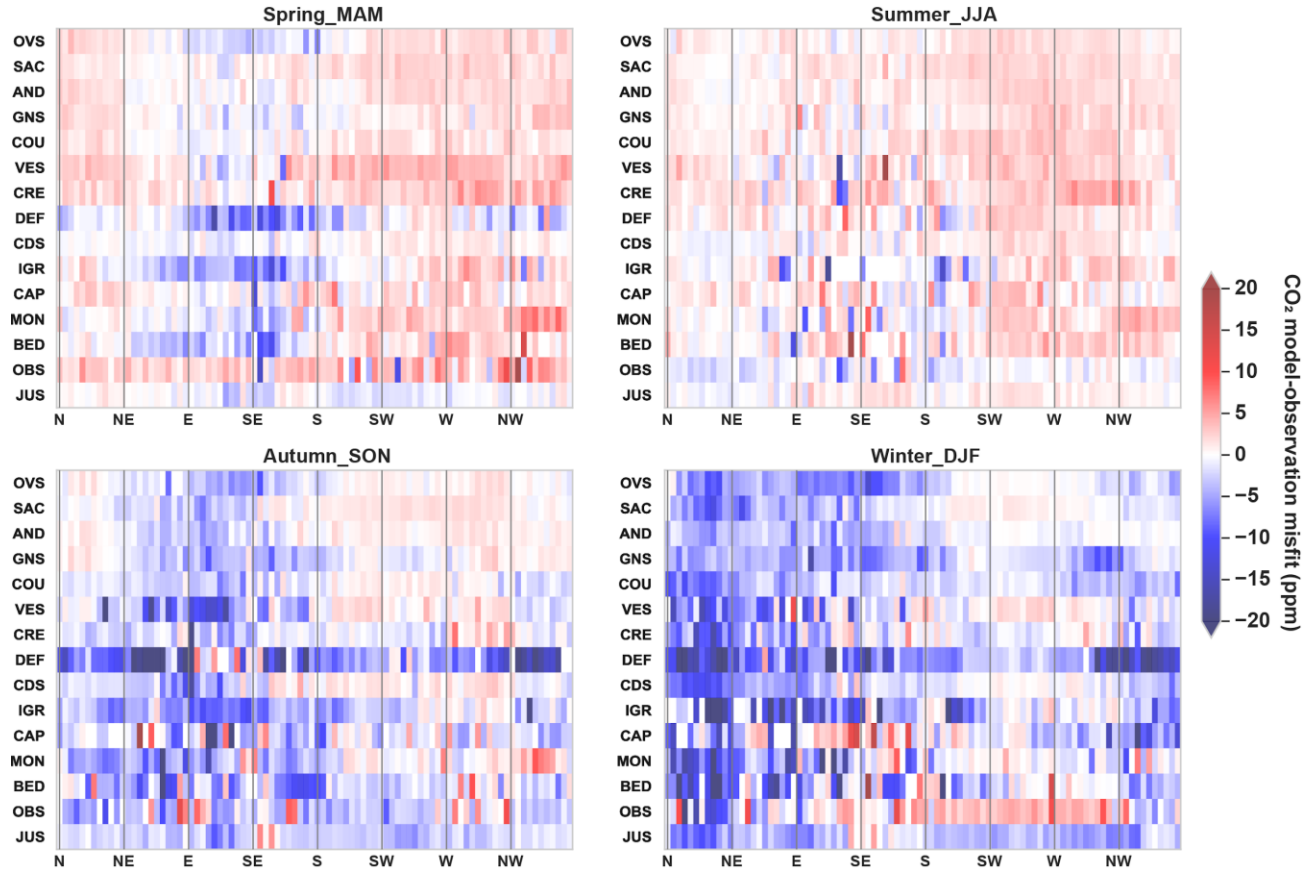

Figure S9. Model-observation misfits in hourly afternoon (12-17 UTC) CO_2 mole fractions, averaged accounting for wind direction for four seasons at 7 CRDS and 8 HPP stations over the period of July 2020 to December 2022. The stations are displayed in a bottom-to-top sequence, corresponding to their increasing distance from the JUS station.

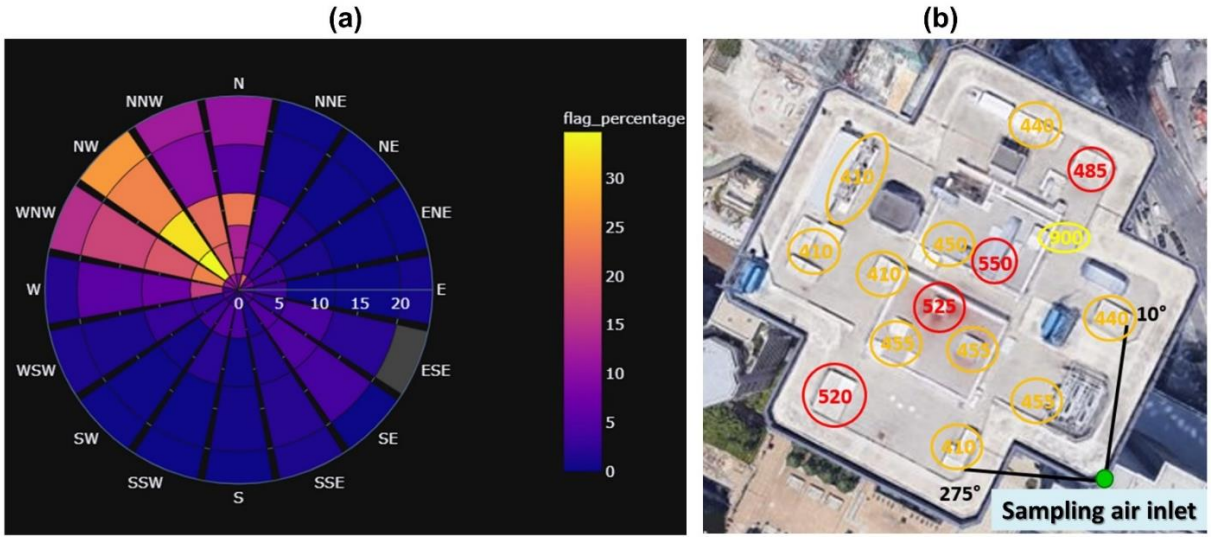

Figure S10. (a) Average spike percentage of observed CO_2 mole fractions as a function of wind speed and direction at DEF station from January to May 2021. (b) A photo of the rooftop at DEF station indicates potential local sources of contamination, primarily originating from the direction spanning 275° to 10°. Red circle: active and high-flow sources of contamination during the visit. Orange circle: potential sources of contamination not active or low flow during the visit. Yellow circle: a source of active contamination but structurally at low flow (e.g., sanitary facilities). Green dot: the location of the sampling air inlet. The image in (b) was extracted from © Google Maps.

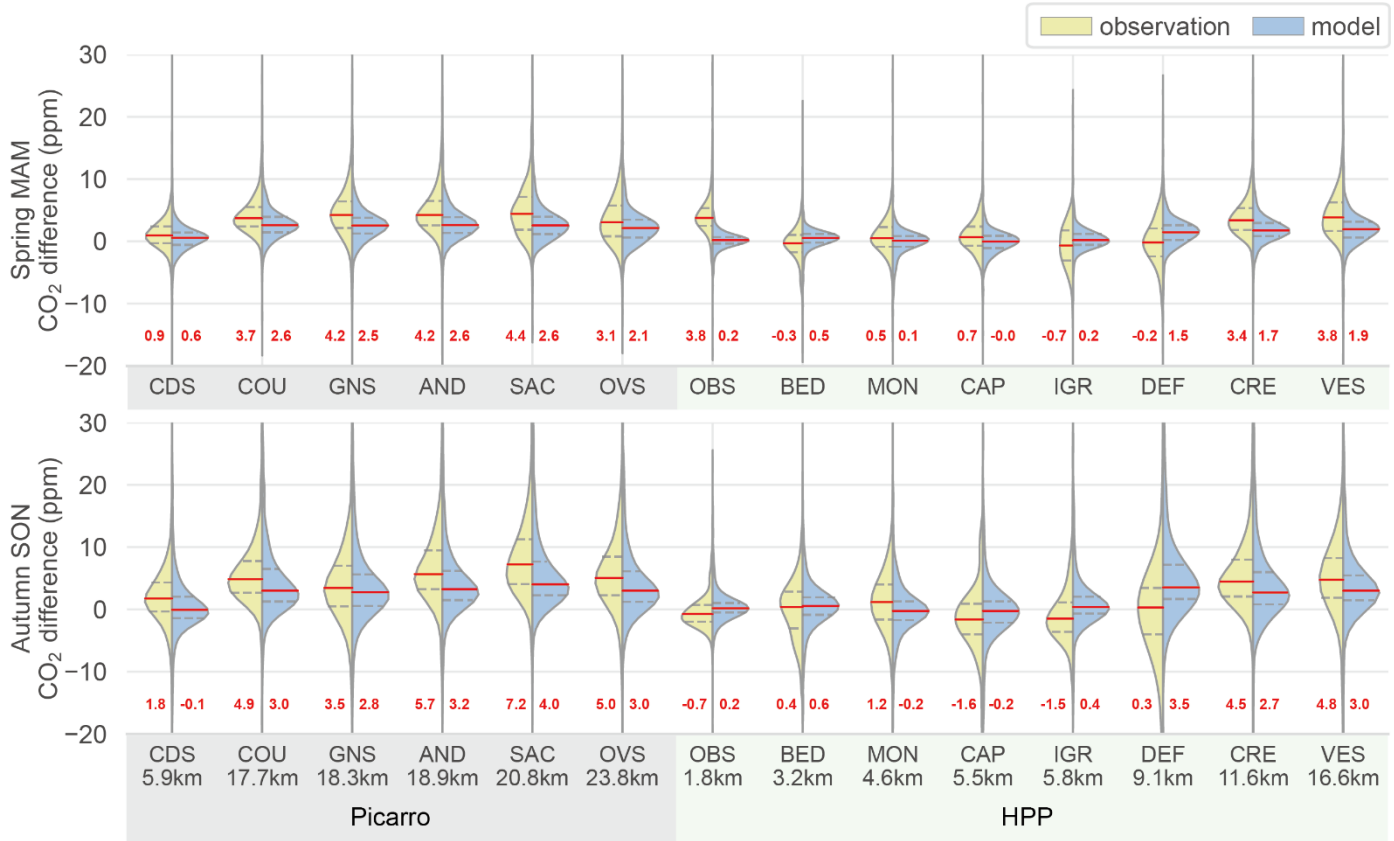

Figure S11. Distributions of the observed and modeled hourly afternoon (12-17 UTC) CO2 mole fraction differences between JUS and the other stations for spring and autumn, spanning from July 2020 to December 2022. The red solid lines and numbers represent the median values. The dash grey lines represent the first and third quantiles. The distances from each site to the JUS site (in kilometers) are provided on the x-labels.

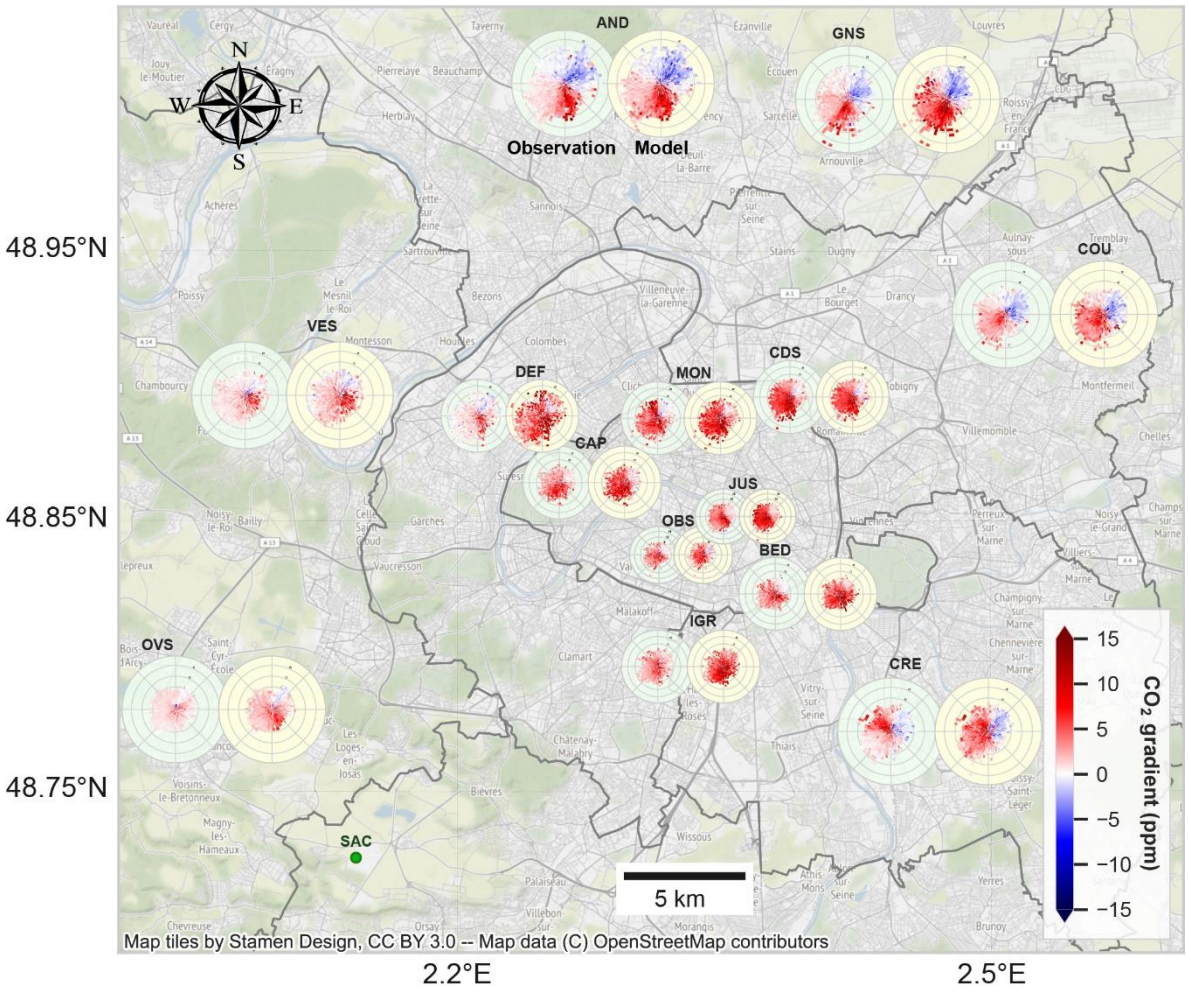

Figure S12. Observed (green panel) and modeled (yellow panel) CO_2 mole fraction differences between all the other stations and SAC, averaged accounting for wind speed and direction over the period of July 2020 to December 2022. Only the afternoon (12-17 UTC) data are used. The CO_2 differences are calculated as the other stations minus SAC. The different sizes of the polar panels hold no specific meaning and are merely adjusted to avoid overlaps.

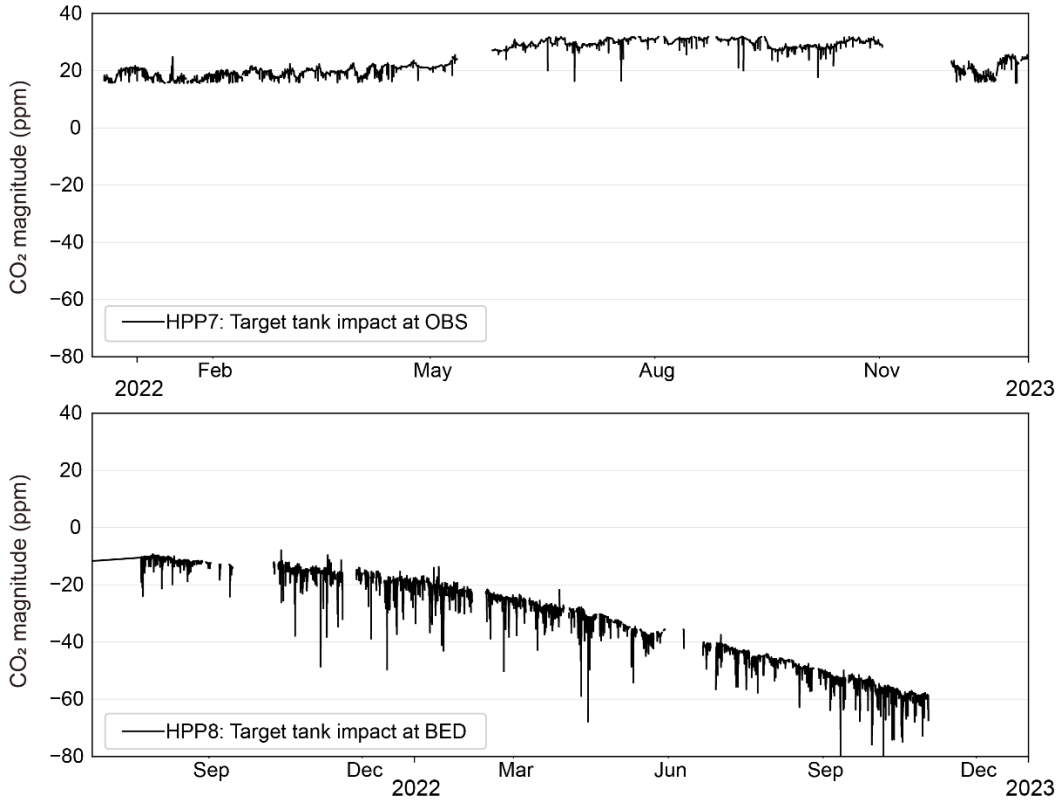

Figure S13. Evolution of the impact of the daily target gas injection in the calibration at two HPP sensors. It was calculated as the CO_2 differences before and after applying $CO_{2_{offset}}$ in Eq. (1).

Table S1. Ranges of acceptable values for critical physical parameters measured by the HPP instrument.

Parameter (unit)	Min value	Max value
H_2O (molar fraction)	0.2%	4%
Pump speed	0.1	0.95
Flowrate (L/min)	0.4	N/A
CO_2 (ppm)	350	700
Detector temperature (°C)	64.98	65.02
Main mirror temperature (°C)	66.90	67.10
Component block temperature (°C)	66.90	67.10
Microcontroller temperature (°C)	0	50